Inorganic Chemistry

Article

pubs.acs.org/IC

Phenylcyanamidoruthenium Scorpionate Complexes

Carmen Harb,[†] Pavel Kravtsov,[†] Mohommad Choudhuri,[†] Eric R. Sirianni,[‡] Glenn P. A. Yap,[‡] A. B. P. Lever,*[,§] and Robert J. Crutchley*[,†]

[†]Department of Chemistry, Carleton University, Ottawa, Ontario K1S 5B6, Canada

[‡]Department of Chemistry and Biochemistry, University of Delaware, Newark, Delaware 19716, United States

[§]Department of Chemistry, York University, Toronto, Ontario M3J 1P3, Canada

Supporting Information

ABSTRACT: Nine [Ru(Tp)(dppe)L] complexes, where Tp is hydrotris(pyrazol-1-yl)borate, dppe is ethylenebis(diphenylphosphine), and L is (4-nitrophenyl)cyanamide (NO_2pcyd$^-$), (2-chlorophenyl)cyanamide (2-Clpcyd$^-$), (3-chlorophenyl)cyanamide (3-Clpcyd$^-$), (2,4-dichlorophenyl)-cyanamide (2,4-Cl_2pcyd$^-$), (2,3-dichlorophenyl)cyanamide (2,3-Cl_2pcyd$^-$), (2,5-dichlorophenyl)cyanamide (2,5-Cl_2pcyd$^-$), (2,4,5-trichlorophenyl)cyanamide (2,4,5-Cl_3pcyd$^-$), (2,3,5,6-tetrachlorophenyl)cyanamide (2,3,5,6-Cl_4pcyd$^-$), and (pentachlorophenyl)cyanamide (Cl_5pcyd$^-$), and the dinuclear complex [{Ru(Tp)(dppe)}$_2$(μ-adpc)], where adpc^{2-} is azo-4,4-diphenylcyanamide, have been prepared and characterized. The crystal structures of [Ru(Tp)(dppe)-(Cl_5pcyd)] and [{Ru(Tp)(dppe)}$_2$(μ-adpc)] reveal the Ru^{II} ion to occupy a pseudooctahedral coordination sphere in which the cyanamide ligand coordinates to Ru^{II} by its terminal nitrogen atom. For both complexes, the cyanamide ligands are planar, indicating significant π mixing between the cyanamide and phenyl moieties as well as the azo group in the case of adpc^{2-}. The optical spectra of the nominally ruthenium(III) species [Ru(Tp)(dppe)L]$^+$ were obtained through spectroelectrochemistry measurements and showed an intense near-IR absorption band. Time-dependent density functional theory calculations of these species revealed that oxidation of the ruthenium(II) species led to species where partial oxidation of the cyanamide ligand had occurred, indicative of noninnocent character for these ligands. The spin densities reveal that while the 3-Clpycd species has substantial Ru^{II}(3-Clpycd^0) character, the Cl_5pycd species is a much more localized ruthenium(III) complex of the Cl_5pycd monoanion. Some bond order and charge distribution data are derived for these ruthenium(III) species. The near-IR band is assigned as a quite complex mixture of d−d, 4d$_\pi$ to L(NCN) MLCT, and L(NCN) to Ru 4d LMCT with even a scorpionate ligand component. Spectroelectrochemistry was also performed on [{Ru(Tp)(dppe)}$_2$(μ-adpc)] to generate the mixed-valence state. The intense intervalence transition that is observed in the near-IR is very similar to that previously reported for [{Ru(trpy)(bpy)}$_2$(μ-adpc)]$^{2+}$, where trpy is 2,2′:6′,2″-terpyridine and bpy is 2,2′-bipyridine, and by analogy identifies [{Ru(Tp)(dppe)}$_2$(μ-adpc)]$^+$ as a delocalized mixed-valence complex.

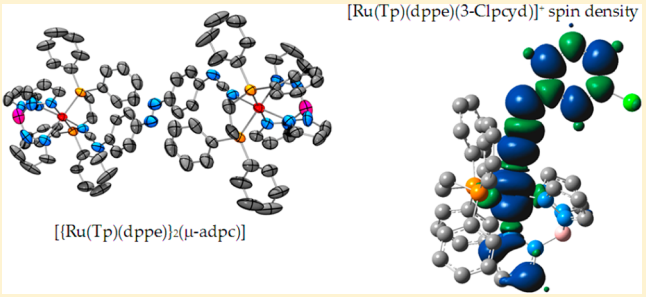

INTRODUCTION

Donor−acceptor polymeric materials have found application in a number of devices such as Mach−Zehnder modulators,[1] solar energy cells,[2] and polymer spintronics.[3] For modulator applications, these materials are usually prepared by doping organic donor−acceptor molecules into a host polymer. Donor−acceptor molecules must be neutral so that, under the influence of a large potential field, their dipole moments cause molecules to align in the host polymer and so express nonlinear-optical properties. In coordination chemistry, there are many examples of dinuclear donor−acceptor systems, otherwise called mixed-valence complexes, that possess properties that could find application in electrooptic polymeric materials except for a significant problem. The vast majority of mixed-valence complexes are charged,[4−6] and making neutral mixed-valence complexes without losing the properties of the desired mixed-valence state is a synthetic challenge.

This study will demonstrate that, by a careful choice of ligands, partial neutralization of the complex charge can occur without a catastrophic loss of mixed-valence properties. The neutral analogues to the complexes [Ru(trpy)(bpy)L]$^+$,[7] where L is a substituted phenylcyanamide ligand, trpy is 2,2′:6′,2″-terpyridine, and bpy is 2,2′-bipyridine, and the dinuclear complex [{Ru(trpy)(bpy)}$_2$(μ-adpc)]$^{2+}$,[8] where adpc^{2-} is azo-4,4′-diphenylcyanamide, will be prepared. Upon oxidation, these complexes possess strong π interactions between Ru^{III} and the cyanamide group, which for the dinuclear complex is the superexchange pathway for metal−metal coupling and results in its mixed-valence properties. In previous studies, we have found[9] that the coordination of anionic π-donor atoms to ruthenium decouples the ruthenium acceptor wave function

Received: November 19, 2012
Published: January 22, 2013

   dx.doi.org/10.1021/ic302535h | Inorg. Chem. 2013, 52, 1621−1630

from the cyanamide superexchange pathway and that this results in weak coupling between metal ions. Neutralization of the complex charge may be achieved by using an anionic auxiliary ligand whose charge is delocalized and so possesses poor π-donor properties. Scorpionate ligands successfully achieve this result.[10] Hydrotris(pyrazol-1-yl)borate (Tp^-) is a commercially available anionic tridentate ligand that coordinates to a metal ion through its pyrazolyl groups. The complex $[Ru(Tp)_2]$ possesses a $Ru^{III/II}$ couple of 0.45 versus normal hydrogen electrode (NHE),[11] which, in comparison with that of other ruthenium homoleptic complexes of ammine and terpyridine, shows that Tp^- stabilizes the Ru^{II} oxidation state better than ammine ($[Ru(NH_3)_6]^{3+/2+}$ = 0.05 V vs NHE) but significantly less than 2,2′;6′,2″-terpyridine ($[Ru(trpy)_2]^{3+/2+}$ = 1.25 V vs NHE).[12] In order to stabilize the Ru^{II} oxidation state further, two coordination sites around Ru^{II} will be occupied by 1,2-bis(diphenylphosphino)ethane (dppe).[13]

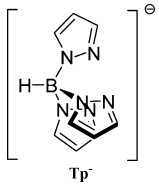

Tp⁻

Nine mononuclear complexes [Ru(Tp)(dppe)L] and a dinuclear complex $[\{Ru(Tp)(dppe)\}_2(\mu\text{-adpc})]$ have been prepared and characterized by ^1H NMR, IR, UV−vis, and near-IR (NIR) spectroscopies, cyclic voltammetry, elemental analysis, and crystallography. Density functional theory (DFT) calculations of the mononuclear ruthenium(III) complexes revealed the electronic properties of the ruthenium cyanamide chromophore. The mixed-valence properties of $[\{Ru(Tp)(dppe)\}_2(\mu\text{-adpc})]^+$ are compared with those of the previously studied ion,[8] $[\{Ru(trpy)(bpy)\}_2(\mu\text{-adpc})]^{3+}$.

EXPERIMENTAL SECTION

Ruthenium(III) chloride trihydrate (reagent grade, Pressure Chemical Co.), triphenylphosphine (PPh_3; ReagentPlus, 99%, Sigma-Aldrich), potassium hydrotris(pyrazol-1-yl)borate hydrate (KTp; 98%, Strem Chemicals), and 1,2-bis(diphenylphosphino)ethane (dppe; 99%, Aldrich) were used as received. Thallium salts of (4-nitrophenyl)-cyanamide (NO_2pcyd^-), (2-chlorophenyl)cyanamide (2-Clpcyd$^-$), (3-chlorophenyl)cyanamide (3-Clpcyd$^-$), (2,4-dichlorophenyl)cyanamide (2,4-Cl_2pcyd$^-$), (2,3-dichlorophenyl)cyanamide (2,3-Cl_2pcyd$^-$), (2,5-dichlorophenyl)cyanamide (2,5-Cl_2pcyd$^-$), (2,4,5-trichlorophenyl)-cyanamide (2,4,5-Cl_3pcyd$^-$), (2,3,5,6-tetrachlorophenyl)cyanamide (2,3,5,6-Cl_4pcyd$^-$), (pentachlorophenyl)cyanamide (Cl_5pcyd$^-$), and azo-4,4-diphenylcyanamide (adpc^{2-}) were prepared from literature methods.[8,14−17] Tetrabutylammonium hexafluorophosphate (TBAH) was synthesized by combining 0.1 M aqueous solutions of tetrabutylammonium bromide (95+%, Aldrich) and ammonium hexafluorophosphate (ReagentPlus, 99%, Sigma-Aldrich). The resulting TBAH powder was twice recrystallized from 1:1 ethanol/water and vacuum-dried at 110 °C. *N*,*N*′-Dimethylformamide (DMF; Sigma-Aldrich, ChromosolvPlus, 99.9%, HPLC grade) was used as received. The reagent complexes $Ru(PPh_3)_3Cl_2$,[18] $Ru(Tp)(PPh_3)_2Cl$,[19] and Ru(Tp)(dppe)Cl[20] were prepared according to literature methods.

Preparation of [Ru(Tp)(dppe)(4-NO_2pcyd)]·0.2CH_2Cl_2. To a 500 mL round-bottomed flask equipped with a stir bar and containing degassed DMF (200 mL) was added [Ru(Tp)(dppe)Cl] (0.500 g, 0.67 mmol) under positive argon pressure. The solution was refluxed under argon until [Ru(Tp)(dppe)Cl] dissolved. Tl[4-NO_2pcyd] (0.245 g, 0.67 mmol, fw 366.36 g/mol) was then added, and the mixture was refluxed for 3 h under argon, during which time the solution changed from dark orange to bright orange and a white precipitate of TlCl formed. After cooling at 4 °C overnight, TlCl was filtered off using a Celite packed column and the filtrate was rotary evaporated to approximately 20 mL. Anhydrous diethyl ether (60 mL) was added to the flask to precipitate out the crude product. The crude product was collected, washed with diethyl ether, and recrystallized from 2:1:1 CH_2Cl_2/ether/hexane first by dissolving the product in a minimum volume of CH_2Cl_2, then by adding diethyl ether using half of that volume, and finally by adding an equivalent volume of hexane. The crystals were collected and dried under vacuum. Yield: 0.327 g (55.9%). IR (KBr pellets): ν(NCN) 2180, ν(BH) 2489 cm^{-1}. ^1H NMR (300 MHz, DMSO-d_6): δ 8.06 (2H, d), 7.78 (1H, d), 7.72 (2H, d), 7.41 and 7.38 (10H, two overlapping br s peaks), 7.24, (2H, t), 7.03 and 7.02 [(4H, t) and (2H, d), overlapping t and d peaks, respectively], 6.75 (4H, t), 6.26 (2H, t), 6.10 (2H, d), 5.76 (CH_2Cl_2 of crystallization, s), 5.45 (1H, d), 5.28 (1H, t), 5.00−4.00 (1H, br s), 3.10 (4H, m). Anal. Calcd for $C_{42.2}H_{38.4}N_9Cl_{0.4}O_2P_2BRu$: C, 56.85; H, 4.34; N, 14.14. Found: C, 57.06; H, 4.31; N, 14.07.

Preparation of [Ru(Tp)(dppe)(2-Clpcyd)]·$^1/_2CH_2Cl_2$. A method analogous to that above was used. Yield: 0.15 g (51.8%). IR (KBr pellets): ν(NCN) 2181, ν(BH) 2481 cm^{-1}. ^1H NMR (300 MHz, DMSO-d_6): δ 8.03 (2H, d), 7.73 (1H, d), 7.42 (10H, overlapping peaks: 2H, t; 4H, t; 4H, t), 7.23 (4H, t), 7.03 (7H, overlapping peaks: 1H, d; 4H, t; 2H, d), 6.70 (5H, overlapping peaks: 1H, t; 4H, t), 6.38 (1H, t), 6.24 (2H, t), 6.04 (1H, d), 5.76 (s), 5.37 (1H, d), 5.24 (1H, t), 4.66 (1H, s), 3.05 (4H, t). Anal. Calcd for $C_{42.5}H_{39}N_8P_2BCl_2Ru$: C, 56.31; H, 4.34; N, 12.36. Found: C, 56.52; H, 3.97; N, 11.96.

Preparation of Ru(Tp)(dppe)(3-Clpcyd)·0.4CH_2Cl_2. A method analogous to that above was used. Yield: 0.17 g (52.1%). IR (KBr pellets): ν(NCN) 2173, ν(BH) 2476 cm^{-1}. ^1H NMR (300 MHz, DMSO-d_6): δ 8.03 (2H, d), 7.73 (1H, d), 7.42 (10H, overlapping peaks: 2H, t; 4H, t; 4H, t), 7.23 (4H, t), 7.03 (6H, overlapping peaks: 4H, t; 2H, d), 6.70 (5H, overlapping peaks: 1H, t; 4H, t), 6.39 (1H, d), 6.23 (2H, t), 6.10 (1H, t), 6.03 (1H, d), 5.76 (s), 5.37 (1H, d), 5.24 (1H, t), 4.65 (1H, s), 3.04 (4H, t). Calcd for $C_{42.4}H_{38.8}N_8P_2BCl_{1.8}Ru$: C, 56.71; H, 4.35; N, 12.48. Found: C, 56.95; H, 4.15; N, 12.23.

Preparation of Ru(Tp)(dppe)(2,3-Cl_2pcyd)·$^1/_2CH_2Cl_2$. A method analogous to that above was used. Yield: 0.14 g (50.4%). IR (KBr pellets): ν(NCN) 2181, ν(BH) 2476 cm^{-1}. ^1H NMR (300 MHz, DMSO-d_6): δ 8.03 (2H, d), 7.73 (1H, d), 7.42 (10H, overlapping peaks: 2H, t; 4H, t; 4H, t), 7.23 (4H, t), 7.03 (6H, overlapping peaks: 4H, t; 2H, d), 6.70 (5H, overlapping peaks: 1H, t; 4H, t), 6.59 (1H, d), 6.25 (2H, t), 5.93 (1H, d), 5.76 (s), 5.37 (1H, d), 5.24 (1H, t), 4.65 (1H, s), 3.04 (4H, t). Calcd for $C_{42.5}H_{38}N_8P_2BCl_3Ru$: C, 54.25; H, 4.07; N, 11.91. Found: C, 54.47; H, 3.88; N, 11.68.

Preparation of Ru(Tp)(dppe)(2,5-Cl_2pcyd)·0.8CH_2Cl_2. A method analogous to that above was used. Yield: 0.16 g (52.3%). IR (KBr pellets): ν(NCN) 2181, ν(BH) 2473 cm^{-1}. ^1H NMR (300 MHz, DMSO-d_6): δ 8.03 (2H, d), 7.73 (1H, d), 7.42 (10H, overlapping peaks: 2H, t; 4H, t; 4H, t), 7.23 (4H, t), 7.03 (7H, overlapping peaks: 1H, d; 4H, t; 2H, d), 6.70 (4H, t), 6.47 (1H, d), 6.02 (1H, s), 5.76 (s), 5.37 (1H, d), 5.24 (1H, t), 4.65 (1H, s), 3.04 (4H, t). Calcd for $C_{42.8}H_{38.6}N_8P_2BCl_{3.6}Ru$: C, 53.19; H, 4.03; N, 11.59. Found: C, 53.09; H, 3.76; N, 11.42.

[Ru(Tp)(dppe)(2,4-Cl_2pcyd)]·CH_2Cl_2. A method analogous to that above was used. Yield: 0.300 g (49.9%). IR (KBr pellets): ν(NCN) 2171, ν(BH) 2486 cm^{-1}. ^1H NMR (300 MHz, DMSO-d_6): δ 8.04 (2H, d), 7.75 (1H, d), 7.41 and 7.39 (10H, two overlapping br s peaks), 7.23 (2H, t), 7.06, 7.05, and 7.04 [(4H, t), (1H, d), and (2H, d) overlapping t, d, and d peaks, respectively], 6.75 and 6.74 [(1H, d) and (4H, m) overlapping d and m peaks, respectively], 6.25 (2H, t), 5.94 (1H, d), 5.76 (CH_2Cl_2 of crystallization, s), 5.39 (1H, d), 5.25 (1H, t), 5.00−4.00 (1H, br s), 3.06 (4H, m). Anal. Calcd for $C_{43}H_{39}N_8Cl_4P_2BRu$: C, 52.52; H, 3.99; N, 11.39. Found: C, 52.89; H, 3.82; N, 11.51.

[Ru(Tp)(dppe)(2,4,5-Cl_3pcyd)]·$^1/_2C_4H_{10}O$. A method analogous to that above was used. Yield: 0.380 g (60.9%). IR (KBr pellets): ν(NCN) 2189, ν(BH) 2473 cm^{-1}. ^1H NMR (300 MHz, DMSO-d_6): δ 8.05 (2H, d), 7.76 (1H, d), 7.39 and 7.36 (10H, two overlapping br s peaks), 7.26 and 7.24 [(1H,s) and (2H, t) overlapping s and t peaks, respectively], 7.04 and 7.02 [(4H, t) and (2H, d) overlapping t and d peaks, respectively], 6.75 (4H, t), 6.24 (2H, t), 6.05 (1H, s), 5.39 (1H,

dx.doi.org/10.1021/ic302535h | Inorg. Chem. 2013, 52, 1621−1630

d), 5.26 (1H, t), 5.00−4.00 (1H, br s), 3.06 (4H, m), 3.39 and 1.09 ($C_4H_{10}O$ of crystallization, q and t peaks, respectively). Anal. Calcd for $C_{44}H_{41}N_8Cl_3O_{0.5}P_2BRu$: C, 54.48; H, 4.26; N, 11.55. Found: C, 54.65; H, 4.15; N, 11.57.

Preparation of [Ru(Tp)(dppe)(2,3,5,6-Cl_4pcyd)]·0.2CH_2Cl_2. A method analogous to that above was used. Yield: 0.362 g (56.0%). IR (KBr pellets): ν(NCN) 2198, ν(BH) 2479 cm^{-1}. ^1H NMR (300 MHz, DMSO-d_6): δ 8.02 (2H, d), 7.72 (1H, d), 7.35 (10H, two overlapping br s peaks), 7.22 (2H, t), 7.05, 7.02, and 7.00 [(4H, t), (2H, d) and (1H, s) overlapping t, d, and s peaks, respectively], 6.73 (4H, t), 6.22 (2H, t), 5.76 (CH_2Cl_2 of crystallization, s), 5.31 (1H, d), 5.22 (1H, t), 5.00−4.00 (1H, br s), 3.04 (4H, br dd). Anal. Calcd for $C_{42.2}H_{35.4}N_8Cl_{4.4}P_2BRu$: C, 51.49; H, 3.62; N, 11.38. Found: C, 51.82; H, 3.81; N, 10.99.

Preparation of [Ru(Tp)(dppe)(Cl_5pcyd)]. A method analogous to that above was used. Yield: 0.352 g (52.5%). IR (KBr pellets): ν(NCN) 2188, ν(BH) 2459 cm^{-1}. ^1H NMR (300 MHz, DMSO-d_6): δ 8.03 (2H, d), 7.73 (1H, d), 7.35 (10H, two overlapping br s peaks), 7.23 (2H, t), 7.05 and 7.02 [(4H, t) and (2H, d), overlapping t and d peaks, respectively], 6.73 (4H, t), 6.22 (2H, t), 5.33 (1H, d), 5.23 (1H, t), 5.00−4.00 (1H, br s), 3.04 (4H, br dd). Anal. Calcd for $C_{42}H_{34}N_8Cl_5P_2BRu$: C, 50.35; H, 3.42; N, 11.18. Found: C, 50.08; H, 3.16; N, 11.11.

Preparation of [{Ru(Tp)(dppe)}$_2$(μ-adpc)]·DMF·2H_2O. To a 500 mL round-bottomed flask equipped with a stir bar and degassed DMF (200 mL) was added [Ru(Tp)(dppe)Cl] (0.500g, 0.67 mmol) under argon. The solution was refluxed and stirred until [Ru(Tp)-(dppe)Cl] dissolved. Under positive argon pressure, Tl_2[adpc] (0.223 g, 0.33 mmol) was then added, and the mixture was refluxed overnight. The dark-red reaction mixture was filtered through a Celite packed column in order to separate the fine TlCl particles, the filtrate was rotary evaporated to a minimum volume, and the product complex precipitated by ether diffusion. Yield: 0.500 g (88.7%). IR (KBr pellets): ν(NCN) 2174, ν(BH) 2470 cm^{-1}. ^1H NMR (300 MHz, DMSO-d_6): δ 8.04 (4H, d), 7.75 (2H, d), 7.43 and 7.42 (20H, two overlapping br s peaks), 7.31 (4H, d), 7.23 (4H, t), 7.07 (4H, d), 7.04 (8H, t), 6.76 (8H, t), 6.25 (4H, t), 6.18 (4H, d), 5.38 (2H,d), 5.25 (2H, t), 5.00−4.00 (2H, br s), 3.32 (H_2O associated with the complex), 3.06 (8H, m), 7.95, 2.89, and 2.73 (DMF of crystallization, three singlet peaks). Anal. Calcd for $C_{87}H_{87}N_{19}O_3P_4B_2Ru_2$: C, 58.23; H, 4.88; N, 14.83. Found: C, 58.32; H, 4.68; N, 14.48.

PHYSICAL MEASUREMENTS

BOMEM Michelson MB100 FT-IR and Cary 5 UV−vis−NIR spectrophotometers were used to record IR and electronic spectra, respectively. ^1H NMR spectra of dimethyl-d_6 sulfoxide (DMSO-d_6) solutions were recorded using a Bruker 300 Ultra Shield spectrometer at room temperature. Cyclic voltammetry studies were performed with a Ω Metrohm Autolab PGSTAT30 potentiostat/galvanostat on argon-saturated solutions of the complexes in DMF with 0.1 M TBAH as the supporting electrolyte. A three-electrode arrangement consisting of a platinum disk working electrode (BAS, 1.6 mm diameter), a platinum-wire auxiliary electrode, and a silver-wire quasi-reference electrode was used. The electrochemical cell consisted of a double-jacketed glass container with an internal volume of 15 mL. Ferrocene (E° = 0.665 V vs NHE)[21] and cobaltocenium hexafluorophosphate (E° = −0.589 V vs NHE)[21] were used for calibration.

An optically transparent thin-layer electrochemical cell arrangement was used to conduct spectroelectrochemical studies.[22,23] Indium−tin oxide-coated glass served as working and counter electrodes, and AgCl/Ag was used as the reference electrode. The solvents and supporting electrolyte were the same as those used for cyclic voltammetry. For the spectroelectrochemical studies, the spectroscopic changes observed upon oxidation are reversible with greater than 95% recovery of the original complex spectrum. Elemental analyses were performed by Canadian Microanalytical Services Ltd., Delta, British Columbia, Canada.

Crystallography. Crystals of [RuTp(dppe)(Cl_5pcyd)] and [{RuTp(dppe)}$_2$(μ-adpc)]·2H_2O were grown by slow diffusion of diethyl ether into a concentrated DMF solution of each complex. The diffraction data were collected on a Bruker-AXS Smart Apex CCD diffractometer using Mo Kα radiation (λ= 0.71073 Å) at 200(2) K using an ω-scan technique and corrected for absorption using equivalent reflections. The unit-cell parameters, equivalent reflections, and systematic absences were uniquely consistent for the reported space groups. Direct methods were used to solve the structures, and refinement was carried out with full-matrix least-squares procedures. The diruthenium complex structure was located on an inversion center. Anisotropic refinement was performed on all non-hydrogen atoms. Borate protons were located from the electron density map and refined in position with 1.2U_{eq} of the attached boron atom. All other hydrogen atoms were treated as idealized contributions. Scattering factors are contained in the *SHELXTL*, version 6.12, program library.[24] The data set for [{RuTp(dppe)}$_2$(μ-adpc)]·2H_2O was treated with *SQUEEZE* to model the disordered water molecules of hydration as diffused contributions.[25] CIF documents for both complexes have been deposited with the CSD under depositary numbers 900736 and 900737.

Oscillator Strength Calculation. Because of the non-Gaussian ligand-to-metal charge-transfer (LMCT) band shape, calculation of the oscillator strength using eq 1,[26]

$$f = 4.61 \times 10^{-9} \varepsilon_{max} \Delta\nu_{1/2} \quad (1)$$

where ε_{max} is the maximum extinction coefficient in M^{-1} cm^{-1} and $\Delta\nu_{1/2}$ is the bandwidth at half-peak-height in cm^{-1}, would lead to an inexact value. In order to obtain a more accurate value, multiple Gaussian bands were fitted to the NIR band envelope using Jandel Scientific *Peakfit v3.0* software. A representative fit is shown in the Supporting Information (Figure S1). The NIR band oscillator strength was then calculated according to eq 2, which sums the oscillator strength from each of the Gaussian bands to give the total oscillator strength of the NIR transition.

$$f = 4.61 \times 10^{-9} \sum_i \varepsilon_i \Delta\nu_i \quad (2)$$

In the above equation, ε_i and $\Delta\nu_i$ are the extinction coefficient at λ_{max} and bandwidth at half-peak-height in cm^{-1}, respectively, of each Gaussian band.

DFT Calculations. DFT calculations utilized the *Gaussian 09* (revisions B.01 and C.01) program.[27] Optimized geometries were calculated using the B3LYP exchange-correlation functional[28] with the LANL2DZ basis set[29−31] for all elements except ruthenium, chlorine, and phosphorus, for which the def2-TZVP triple-ζ basis set was used.[32] Tight self-consistent-field convergence criteria (10^{-8} au) were used for all calculations. The wave functions were stable (checked with Stable keyword), and the stationary points were truly minima (Freq keyword check).

Molecular orbital (MO) compositions were calculated using the *AOMix* program[33,34] using the Mulliken scheme.[32,35−38] Atomic charges were calculated using the Mulliken[35−38] and natural population analysis[39] methods (MPA and NPA, respectively), as implemented in *Gaussian 09*, revisions B.01

dx.doi.org/10.1021/ic302535h | *Inorg. Chem.* 2013, 52, 1621−1630

and C.01. Extended charge decomposition analysis was performed using *AOMix-CDA*.[34,40] The PCM[41,42] was used to model solvation for methanol as the solvent.

Time-dependent DFT (TD-DFT)[43−45] was used to calculate the energies and intensities of the 80 lowest-energy electronic transitions of both complexes. These were converted with the *SWizard* program[46] into simulated spectra using Gaussian functions with half-widths of 2500 cm^{-1}.

RESULTS AND DISCUSSION

For this study, mononuclear and dinuclear complexes were synthesized under argon to avoid oxidation, and it was important to ensure that the reagent complex [Ru(Tp)(dppe)-Cl] was completely dissolved before the addition of the cyanamide thallium salt; otherwise, yields were significantly less, and the product was difficult to purify. Mononuclear complexes were, for the most part, readily soluble in organic solvents. However, with increasing numbers of chloro substituents on the phenylcyanamide ligand, slight heating was required for dissolution. ^{1}H NMR spectra of the complexes showed chemical shifts (see the Experimental Section) belonging to Tp, dppe, and phenylcyanamide ligands with integrations consistent with the complex stoichiometry. In the case of (pentachlorophenyl)cyanamide complex, the presence of the cyanamide ligand was confirmed by the strong ν(NCN) band observed in the complex's IR spectrum. The ν(NCN) band is observed in the range of 2171−2198 cm^{-1} for the complexes of this study.

Crystallographic data for the complexes [Ru(Tp)(dppe)-(Cl_5pcyd)] and [{Ru(Tp)(dppe)}$_2$(μ-adpc)] are given in Table 1, and Figures 1 and 2 show ORTEP drawings of the complexes, respectively. Tables 2 and 3 present the bond lengths and angles for [Ru(Tp)(dppe)(Cl_5pcyd)] and [{Ru-(Tp)(dppe)}$_2$(μ-adpc)], respectively. For both complexes, the Ru^{II} ions occupy a pseudooctahedral coordination sphere in which the cyanamide moiety coordinates to Ru^{II} by its terminal nitrogen atom and the cyanamide moiety is approximately in the plane of the phenyl ring of the cyanamide ligand. The planarity of the phenylcyanamide and adpc ligands has been observed in other crystal structures and is ascribed to π mixing between the cyanamide and phenyl π systems.[8,15] In Tables 2 and 3, the cyanamide moiety is approximately linear, as is the angle describing coordination of its terminal nitrogen atom to Ru^{II}. This may suggest significant π interactions, but when the coordination sphere is not sterically constrained, smaller bond angles have been observed. For example, [Pd(trpy)(2,6-dichlorophenylcyanamide)]$^+$ possesses a Pd^{II}−NCN bond angle of 137.9(4)°.[47] Ruthenium(II) cyanamide bond lengths in Tables 2 and 3 are similar to those seen in other ruthenium(II) complexes.[7,48]

Table 4 gives the $Ru^{III/II}$ couples of the mononuclear [Ru(Tp)(dppe)L] complexes, where L is a substituted phenylcyanamide ligand, as well as the vis−NIR electronic absorption data for [Ru(Tp)(dppe)L]$^{0,+}$. Cyclic voltammetry of the [Ru(Tp)(dppe)L] complexes showed a single reversible wave in the range of 0.7−1 V. This couple shifts to more positive potentials with increasing numbers of chloro substituents on the phenylcyanamide ligand, which is consistent with an overall reduction of ligand donor properties. The formal assignment of this wave to a $Ru^{III/II}$ couple is complicated by the noninnocence of the cyanamide ligand. Oxidation of [Ru(Tp)(dppe)L] generates an intense NIR band (Table 4 and Figure 3) similar to that seen in other ruthenium cyanamide complexes and previously assigned to a LMCT of the ruthenium(III) cyanamide chromophore.[7,49] However, for the complexes of this study (Table 4), the oscillator strength of

Table 1. Crystal Data and Structure Refinement for [Ru(Tp)(dppe)(Cl_5pcyd)] and [{RuTp(dppe)}$_2$(μ-adpc)]·2H_2O

empirical formula	$C_{42}H_{34}BC_{15}N_8P_2Ru$	$C_{84}H_{80}B_2N_{18}O_2P_4Ru_2$
fw (g/mol)	1001.84	1721.30
temperature (K)	200(2)	200(2)
wavelength (Å)	0.71073	0.71073
cryst syst	orthorhombic	monoclinic
space group	*Pccn*	*P*2(1)/*n*
unit cell dimensions		
a (Å)	20.198(4)	12.035(3)
b (Å)	25.050(5)	25.181(6)
c (Å)	16.714 (4)	15.913(4)
α (deg)	90.00	90.00
β (deg)	90.00	109.513(5)
γ (deg)	90.00	90.00
volume (Å^3), *Z*	8456(3), 8	4545.3(18), 2
density (calcd) (Mg/m^3)	1.574	1.258
abs coeff (mm^{-1})	0.806	0.456
F(000)	4080	1768
cryst size	0.22 × 0.22 × 0.11	0.16 × 0.11 × 0.03
θ range for data collection (deg)	2.27−15.40	2.42−17.36
limiting Indices	$-26 \le h \le 26, -33 \le k \le 30, -22 \le l \le 22$	$-14 \le h \le 14, -29 \le k \le 29, -18 \le l \le 18$
reflns collected	10491	8006
indep reflns	5450 [*R*(int) = 0.0573]	4593 [*R*(int) = 0.0685]
abs corrn	multiscan	multiscan
max and min transmn	0.9166 and 0.8426	0.9878 and 0.9306
refinement method	full-matrix least-squares on F^2	full-matrix least-squares on F^2
data/restraints/ parameters	5450/0/535	8006/0/499
GOF on F^2	1.001	1.023
R1[a]	0.0573	0.0685
wR2[b]	0.1428	0.1280

[a] $R1 = \sum||F_o| - |F_c||/\sum|F_o|$. [b] $wR2 = (\sum w(|F_o| - |F_c|)^2/\sum w|F_o|^2)^{1/2}$.

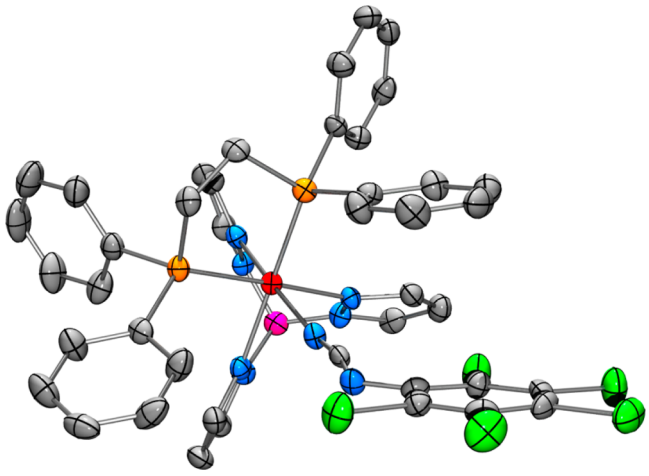

Figure 1. ORTEP diagram of [Ru(Tp)(dppe)(Cl_5pcyd)] with 50% probability ellipsoids. Hydrogen atoms are omitted for clarity. Color code: Ru, red; P, orange; N, blue; B, pink; C, gray; Cl, green.

dx.doi.org/10.1021/ic302535h | *Inorg. Chem.* 2013, 52, 1621−1630

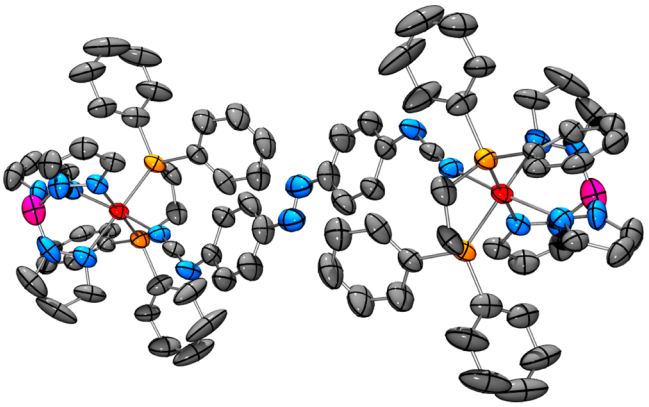

Figure 2. ORTEP diagram of $[\{RuTp(dppe)\}_2(\mu\text{-adpc})]\cdot 2H_2O$ with 50% probability ellipsoids. Water molecules of hydration and hydrogen atoms are omitted for clarity. The color legend is as in Figure 1.

this NIR band decreases with increasing π-donor properties of the cyanamide ligand, while for $[Ru(NH_3)_5L]^{2+}$[15] and dinuclear $[\{Ru(NH_3)_5\}_2(\mu\text{-dicyd})]^{4+}$ complexes,[22] the ruthenium(III) cyanamide NIR band oscillator strength increased with increasing donor properties of the cyanamide group and the strength of ruthenium(III) cyanamide π bond.

To obtain further insight into these species, DFT[50] calculations were carried out on the two extreme members of the mononuclear complexes, [Ru(Tp)(dppe)L], where L = 3-Clpcyd$^-$ and Cl_5pcyd$^-$, henceforth, for simplicity, referred to as the monochloro and pentachloro cyanamide species. To provide as accurate an assessment as possible, consistent with computer cost and time, we employed the B3LYP functional, which behaves well with ruthenium species,[51] and the LANL2DZ basis set for all atoms except ruthenium, phosphorus, and chlorine, where the triple-ζ def2-TZVP basis set, downloaded from EMSL,[32,52] was used. The resulting bond distances agreed well with those expected based on the X-ray structural data (see the Supporting Information), e.g., $d(Ru^{III}$–NCN) = 1.95 Å (monochloro) and 1.96 Å (pentachloro) compared with an average of 1.97 Å observed in six similar ruthenium(III) complexes.[15,17,53] Of particular note, one of the imidazole rings of the scorpionate ligand lies exactly in the plane of the dicyanamide ligand in the DFT-optimized geometry. This is not observed in the X-ray structure of the ruthenium(II) species perhaps because of packing forces or weaker interligand coupling via ruthenium.

As will be discussed in detail below, the TD-DFT calculations of the optical spectra of these two species provide excellent agreement with the experimental UV–vis energies of these two species albeit TD-DFT predicts too high an intensity, which we have previously noted.[54]

The percent composition of the frontier molecular orbitals provides insight into how these systems are constructed at the electronic molecular level. These α and β manifolds are shown in Figures 4 and 5.

The α-HOMO orbital in both complexes is comprised of a π-antibonding interaction between Ru 4dπ and the HOMO of the NCN ligand (specified as HOFO, the HOMO of the fragment NCN ligand). It is the locus of the unpaired electron having an overlap of 0.91 (mono, 0.84 penta) with the β-LUMO of the complex.

The α-LUMO in both species is, somewhat unexpectedly, the σ* antibonding interaction between Ru 4d and two phosphorus and two scorpionate nitrogen atoms.

Of particular relevance is the β-LUMO of these species. This is comprised primarily of an antibonding interaction between the Ru 4dπ β hole and the HOFO of the NCN ligand (Table 5). The corresponding bonding interaction is the β-HOMO in the monochloro species but is the β-HOMO−1 in the pentachloro species. These are strongly mixed Ru 4dπ and π-L(NCN) orbitals and are important for the bonding between ruthenium and L(NCN). This important bonding contribution provided by the β manifold is absent from the α manifold because there is no α-4dπ hole. This then explains why the Mayer bond order between Ru 4d and the NCN ligand is much greater in the β manifold than the α manifold (Table 5). This is not reflected in the Mayer bond orders with the other two ligands because, as shown in Figures 4 and 5, there is little involvement of these ligand orbitals with the β-4dπ hole.

The significantly larger contribution of the L(NCN) HOFO to the β-LUMO in the monochloro species (41.9%) relative to the pentachloro species (33.1%) argues for much greater covalency in the former. This is supported by the spin densities (NPA) shown in Table 6. The L(NCN) ligand is non-innocent,[55] and when the parent ruthenium(II) species is oxidized, there is also partial oxidation of the L(NCN) ligand. Thus, the net single spin is shared almost equally between ruthenium and L(NCN) in the monochloro species but is much more localized on ruthenium in the pentachloro species. Figure 6 shows the MPA spin density of the monochloro species (that for the pentachloro species is shown in the

Table 2. Selected Crystal Structure Data for [Ru(Tp)(dppe)(Cl_5pcyd)]

		Bond Lengths/Å[a]			
Ru–N(7)	2.040(4)	Ru–P(1)	2.2812(13)	N(7)–C(36)	1.173(5)
Ru–N(1)	2.089(3)	Ru–P(2)	2.2878(13)	N(8)–C(36)	1.296(6)
Ru–N(5)	2.131(3)			N(8)–C(42)	1.361(5)
Ru–N(3)	2.134(4)				
		Bond Angles/deg[a]			
N(7)–Ru–N(5)	88.87(13)	N(1)–Ru–P(1)	92.28 (10)	C(36)–N(7)–Ru	166.2(4)
N(1)–Ru–N(5)	85.03(13)	N(5)–Ru–P(1)	97.63(10)	C(36)–N(8)–C(42)	127.4(4)
N(7)–Ru–N(3)	88.68(14)	N(7)–Ru–P(2)	93.58(10)	N(7)–C(36)–N(8)	166.0(5)
N(1)–Ru–N(3)	88.73(13)	N(1)–Ru–P(2)	92.41(10)		
N(5)–Ru–N(3)	83.39(13)	N(3)–Ru–P(2)	93.80(10)		
N(7)–Ru–P(1)	90.40(10)	P(1)–Ru–P(2)	85.22(4)		

[a]Estimated standard deviations are in parentheses.

dx.doi.org/10.1021/ic302535h | Inorg. Chem. 2013, 52, 1621–1630

Table 3. Selected Crystal Structure Data for $[\{RuTp(dppe)\}_2(\mu\text{-adpc})]\cdot 2H_2O$

		Bond Lengths/Å[a]			
Ru–N(7)	2.043(5)	Ru–P(1)	2.2826(18)	N(7)–C(36)	1.155(7)
Ru–N(1)	2.092(5)	Ru–P(2)	2.2628(18)	N(8)–C(36)	1.288(8)
Ru–N(5)	2.122(5)			N(8)–C(42)	1.378(7)
Ru–N(3)	2.132(6)			N(9)–C(39)	1.522(9)
				N(9)–N(9A)	1.154(10)
		Bond Angles/deg[a]			
N(7)–Ru–N(5)	86.8(2)	N(1)–Ru–P(1)	92.82(14)	C(36)–N(7)–Ru	160.6(6)
N(1)–Ru–N(5)	85.83(19)	N(7)–Ru–P(2)	94.61(15)	C(36)–N(8)–C(42)	120.8(5)
N(7)–Ru–N(3)	85.5(2)	N(1)–Ru–P(2)	92.36(15)	N(7)–C(36)–N(8)	172.4(7)
N(1)–Ru–N(3)	87.5(2)	N(3)–Ru–P(1)	95.10(16)	N(9A)–N(9)–C(39)	107.6(9)
N(5)–Ru–N(3)	84.1(2)	N(5)–Ru–P(2)	95.61(14)		
N(7)–Ru–P(1)	94.45(15)	P(2)–Ru–P(1)	85.19(6)		

[a]Estimated standard deviations are in parentheses.

Table 4. Cyclic Voltammetry, NIR, and Absorption Data for $[Ru(Tp)(dppe)L)]^{0,+}$ Complexes

	[Ru(Tp)(dppe)L)]		[Ru(Tp)(dppe)L)]$^+$
L	[Ru(Tp)(dppe)L)]$^{0/+}$ (V)	MLCT[b]	LMCT[b]
2-Clpcyd$^-$	0.72	377 (1720)	1120 (4510) [0.078]
3-Clpcyd$^-$	0.78	375 (2120)	951 (4000) [0.076]
2,4-Cl_2pcyd$^-$	0.80	382 (1400)	997 (4460) [0.076]
2,3-Cl_2pcyd$^-$	0.82	372 (2100)	973 (4930) [0.092]
2,5-Cl_2pcyd$^-$	0.84	377 (2180)	967 (7470) [0.13]
2,4,5-Cl_3pcyd$^-$	0.87	383 (1690)	987 (8700) [0.17]
2,3,5,6-Cl_4pcyd$^-$	0.87	379 (sh, 2600)	929 (9390) [0.17]
Cl_5pcyd$^-$	0.89	379 (sh, 5140)	956 (10700) [0.19]
4-NO_2pcyd$^-$	0.93	457 (2590)[c]	946 (13100) [0.20]

[a]vs NHE, DMF solution, and 0.1 M TBAH. [b]λ_{max} in nm (ε_{max} in M^{-1} cm^{-1}) [oscillator strength f]; sh = shoulder; DMF solution. [c]Mostly intraligand charge transfer.

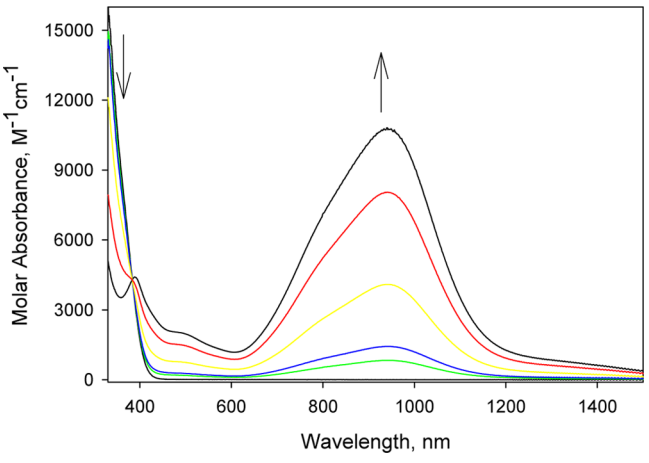

Figure 3. Spectroelectrochemistry of [Ru(Tp)(dppe)(Cl_5pcyd)] in DMF, 0.1 M TBAH, under increasing oxidation potentials (0–0.6 V vs AgCl/Ag).

Supporting Information). It is very similar in appearance to the π-HOMO, which is the SOMO in this complex.

These oxidized species are then visualized as resonance hybrids between Ru^{III}–$L(NCN)^-$ and Ru^{II}–$L(NCN)^0$, with the latter more important in the monochloro species and the former more important in the pentachloro species. This is also seen clearly in the occupancies of the L(NCN) β-HOFO (Table 5), being substantially less than 1 and indeed approaching 0.5 in the monochloro species; i.e., the ligand is close to being described as $L(NCN)^0$.

Thus, the covalent bonding between the metal and L(NCN) ligand is greater in the monochloro species than in the pentachloro species. In terms of the discussion above about the intensity of the visible region absorption, greater mixing between Ru 4dπ and π^* L(NCN) in the primary donor and acceptor MOs involved in the NIR transition, in the monochloro species, will lead to a reduction in the degree of net charge transfer and, hence, a weaker transition intensity in the monochloro species relative to the pentachloro species, as is indeed observed.

The experimental UV–vis and predicted TD-DFT spectra are shown in Figure 7. There is excellent agreement, between theory and experiment, insofar as the energies and band envelope are concerned, but the TD-DFT greatly overemphasizes the intensities especially for the monochloro species. Such predicted enhanced intensities are not unusual.[54] We suppose that the energy/band shape agreement does provide evidence that def2-TZVP DFT analysis is sound. We note in passing that a somewhat poorer fit between the experimental and TD-DFT predicted spectra is noted if LANL2DZ is used for phosphorus and chlorine instead of def2-TZVP. It is especially important in the pentachloro species to use def2-TZVP for chlorine.

The detailed assignments are shown in the Supporting Information in Table S1. The very intense visible region transition is β-HOMO−1 to β-LUMO in the pentachloro species and β-HOMO to β-LUMO in the monochloro species. Although excitation occurs from a different frontier molecular orbital, in fact, β-HOMO−1 (pentachloro) and β-HOMO (monochloro) involve primarily the *same* β-HOFO of the L(NCN) ligand, which is also the primary orbital in β-LUMO. Because the same ligand orbital is involved in both the ground and excited states, overlap is considerable, hence leading to an intense transition. Different 4d orbitals are involved in the ground and excited states (see the Supporting Information). Further, we recall that β-HOFO of the L(NCN) ligand is only

dx.doi.org/10.1021/ic302535h | Inorg. Chem. 2013, 52, 1621–1630

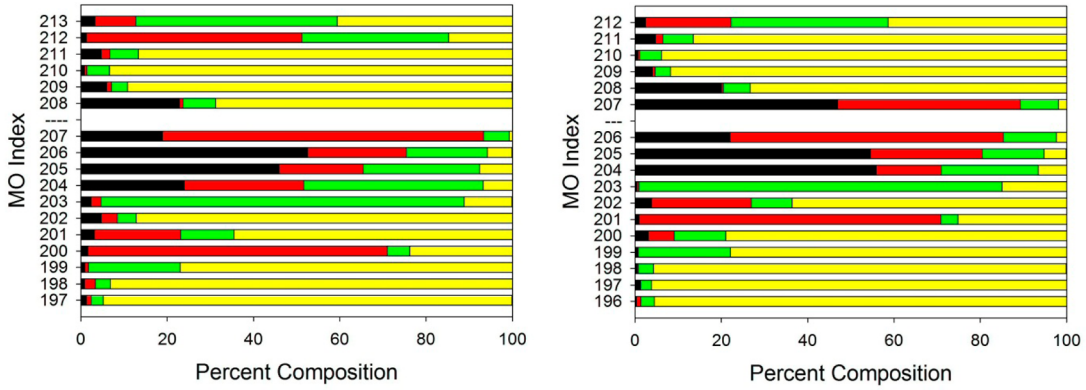

Figure 4. Percent composition of frontier molecular orbitals of monochloro species: α manifold (left); β manifold (right). Color code: Ru, black; NCN ligand, red; scorpionate ligand, green; diphosphine ligand, yellow. The white space identified by --- is the HOMO−LUMO gap. The α-HOMO is 207, and the β-HOMO is 206.

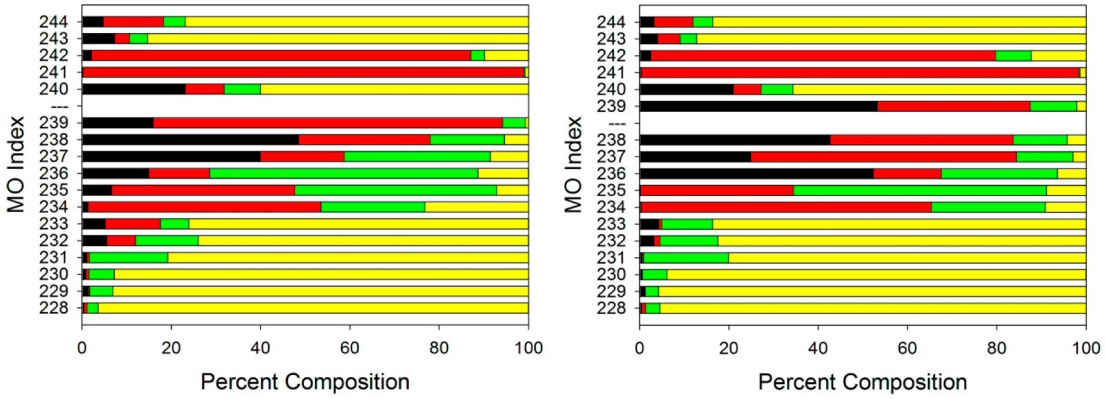

Figure 5. Percent composition of frontier molecular orbitals of pentachloro species: α manifold (left); β manifold (right). Color code: Ru, black; NCN ligand, red; scorpionate ligand, green; diphosphine ligand, yellow. The white space identified by --- is the HOMO−LUMO gap. The α-HOMO is 239, and the β-HOMO is 238.

Table 5. Selected Properties[a] of the Mono- and Pentachlorocyanamido Species

property	Cl−NCN	Cl_5−NCN
α-Ru−L(NCN) Mayer bond order	0.269 (0.317)[b]	0.280 (0.337)[b]
β-Ru−L(NCN) Mayer bond order	0.67 (0.776)[b]	0.625 (0.697)[b]
α-4d valence population	3.95	3.96
β-4d valence population	3.42	3.35
α-HOFO L(NCN) occupancy[c]	97.5	97.4
β-HOFO L(NCN) occupancy[c]	55.7	64.6
% 4d Ru contribution to the β-LUMO[e]	46.9[d]	53.2[d]
% L(NCN) contribution to the β-LUMO[e]	42.3	34.2

[a]DFT calculations, using b3lyp/def2-tzvp for chlorine, phosphorus, and ruthenium atoms. PCM = DMF. [b]Interfragment Mayer bond order between the L(NCN) ligand fragment and the rest of the molecule. [c]39 in the mono species; 71 in the penta species. [d]β hole in Ru 4dπ. [e]See Figures 5 and 6.

Table 6. NPA Spin Densities and Charges[a,b] of the Mono- and Pentachlorocyanamide Species

location	Cl−NCN	Cl_5−NCN
ruthenium	0.54 (−0.45)	0.62 (−0.40)
NCN	0.42 (−0.16)	0.33 (−0.26)
scorpionate	0.05 (0.21)	0.07 (0.22)
diphosphine	−0.02 (1.34)	−0.02 (1.43)

[a]Spin (charge). [b]DFT calculations using b3lyp/def2-tzvp for phosphorus, chlorine, and ruthenium atoms. PCM = DMF.

partially occupied. Thus, this transition can be defined as a mixture of d−d, L(NCN) to Ru 4d LMCT, and indeed 4d to L(NCN) metal-to-ligand charge-transfer (MLCT), thus not easily described! We also note from Figures 4 and 5 that the scorpionate ligand contributes to the relevant MOs and so is involved in this transition.

While DFT analysis reveals only one electronic transition in the region around 12000 cm^{-1}, the experimental envelope clearly indicates extra absorption on the high-energy side. This is most likely due to one or more vibronic transitions where the electronic state is coupled to an ν(NCN) vibration.

At higher energy, broad absorption is seen arising from multiple transitions, many of which, below 30000 cm^{-1}, terminate on the same β-LUMO and originate from scorpionate and diphosphine ligand orbitals, i.e., ligand-to-ligand charge transfer. They tend to be weak because the ligand−ligand overlap is small.

As shown by DFT calculations, oxidation of the ruthenium(II) complexes of this study leads to species where partial oxidation of the cyanamide ligand has occurred, indicative of the noninnocent character for these ligands. The degree of cyanamide ligand oxidation depends upon the relative stability of the cyanamide ligand and the ruthenium ion. For the easily oxidized 1,4-dicyanamidebenzene dianion ($dicyd^{2-}$) and its substituted derivatives,[17] DFT calculations showed that it is

dx.doi.org/10.1021/ic302535h | Inorg. Chem. 2013, 52, 1621−1630

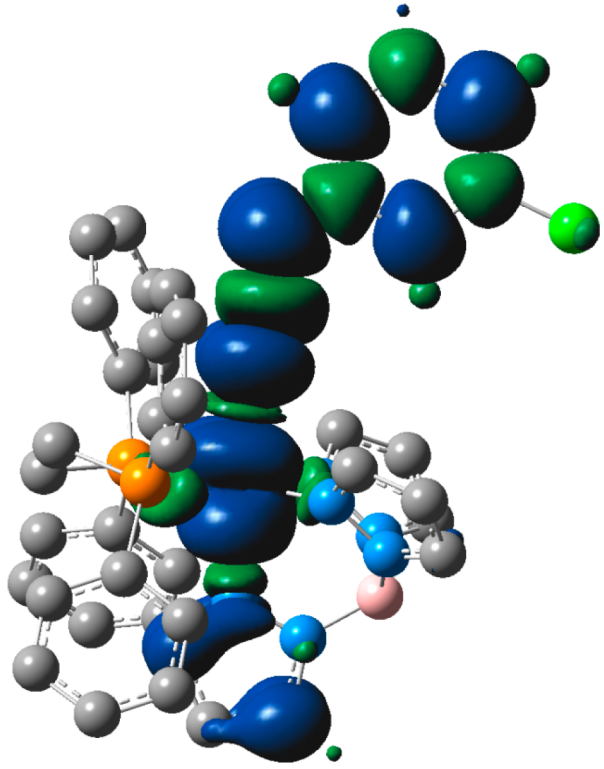

Figure 6. MPA spin density for the monochloro species.

only because of a strong solvation of the $[\{Ru(NH_3)_5\}_2(\mu\text{-dicyd})]^{3+}$ complex that the Ru^{III} ion predominates instead of radical anion $dicyd^{-}$.[56] In contrast, the complex ion $[\{Ru(trpy)(thd)\}_2(\mu\text{-dicyd})]^{+}$, where thd^{-} is 2,2,6,6-tetramethyl-3,5-heptanedione,[55b] shows an electron paramagnetic resonance (EPR) spectrum of a radical $dicyd^{-}$ bridging ligand and therefore has oxidation states $[Ru^{II}, dicyd^{-}, Ru^{II}]$. The first oxidation of free $adpc^{2-}$ occurs at 0.48 V vs NHE,[8] which is approximately 0.9 V more positive than that of $dicyd^{2-}$. The positive shift in potential is largely due to the electron-withdrawing properties of the azo group of $adpc^{2-}$. Cyclic voltammetry and spectroelectrochemical studies of the dinuclear complex ion $[\{Ru(Tp)(dppe)\}_2(\mu\text{-adpc})]^{+}$ were performed to explore its mixed-valence properties and the effect of the Ru(Tp)(dppe) coordination sphere on metal–metal coupling.

The cyclic voltammogram of $[\{Ru(Tp)(dppe)\}_2(\mu\text{-adpc})]$ (Figure S5 in the Supporting Information) showed two reversible couples at 0.67 and 0.81 V vs NHE (Table 4), and this gives a comproportionation constant of only $K_c = 230$, which is far less than that observed for $[\{Ru(trpy)(bpy)\}_2(\mu\text{-adpc})]^{2+}$ ($K_c = 1.3 \times 10^{13}$).[8] This implies significantly weaker metal–metal coupling for the mixed-valent $[\{Ru(Tp)(dppe)\}_2(\mu\text{-adpc})]^{+}$ complex. However, neutral dinuclear complexes upon oxidation are subject to ion-pairing effects, which reduce the comproportionation constant and therefore make K_c a poor measure of metal–metal coupling. This is illustrated by the electrolyte-dependent comproportionation constant of bis(fulvalene)dinickel, which in dichloromethane gives $K_c = 4.1 \times 10^4$ for a 0.1 M $[NBu_4]Cl$ electrolyte but $K_c = 5.4 \times 10^{12}$ for 0.1 M $[NBu_4][B(C_6F_5)_4]$.[57] A more accurate gauge of metal–metal coupling is derived from spectroelectrochemical studies.

Figure 8 shows the vis–NIR absorption changes associated with the formation of $[\{Ru(Tp)(dppe)\}_2(\mu\text{-adpc})]^{+}$ in DMF.

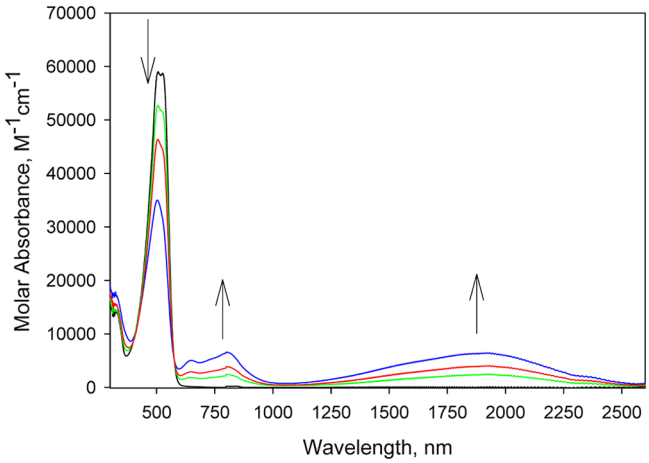

Figure 8. Spectroelectrochemistry of $[\{Ru(Tp)(dppe)\}_2(\mu\text{-adpc})]$ in DMF, 0.1 M TBAH, under increasing oxidation potentials (0.0–0.93 V vs AgCl/Ag).

These spectroscopic changes are strikingly similar to those of $[\{Ru(trpy)(bpy)\}_2(\mu\text{-adpc})]^{3+}$ and strongly suggests that

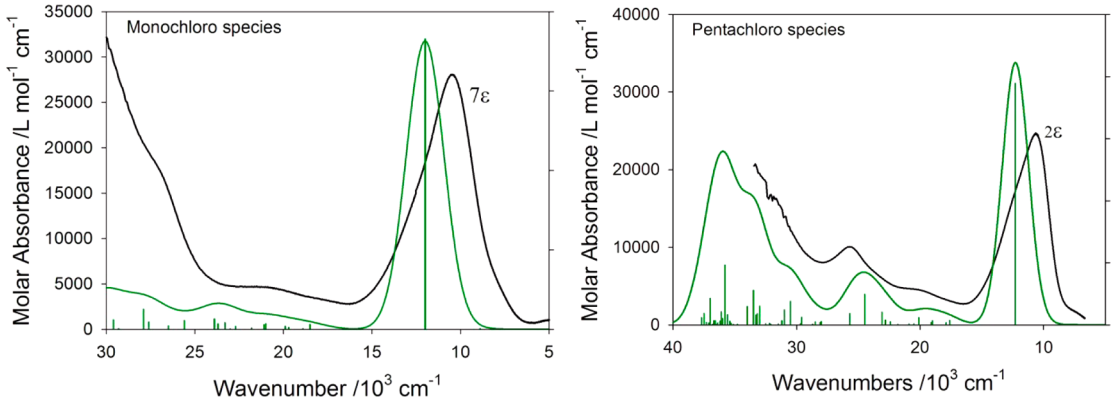

Figure 7. Electronic spectra of the monochloro (left) and pentachloro (right) species. Experimental data recorded in DMF (black) and TD-DFT-calculated spectra (green). Note: The experimental data use the left-hand molar absorbance axis but are multiplied by a factor of 7 for the monochloro species and a factor of 2 for the pentachloro species.

dx.doi.org/10.1021/ic302535h | Inorg. Chem. 2013, 52, 1621–1630

metal−metal coupling in the mixed-valence state is largely unperturbed by a Ru(Tp)(dppe) coordination sphere compared with that of Ru(trpy)(bpy). Indeed, $[\{Ru(Tp)(dppe)\}_2(\mu\text{-adpc})]^+$ shows an intense NIR absorption centered at 1932 nm (ε = 6480 M^{-1} cm^{-1}), which is not much different from the intervalence band of $[\{Ru(trpy)(bpy)\}_2(\mu\text{-adpc})]^{3+}$ (λ_{max} = 1920 nm with ε = 10000 M^{-1} cm^{-1}) in DMF.[8] By analogy with the latter complex, $[\{Ru(Tp)(dppe)\}_2(\mu\text{-adpc})]^+$ is suggested to possess a delocalized mixed-valence state with resonance exchange integral H_{ad} = 2600 cm^{-1} (half of the energy of the intervalence transition).[58]

CONCLUSION

Nine mononuclear [Ru(Tp)(dppe)L] complexes, where L is a substituted phenylcyanamide ligand, and the dinuclear complex $[\{Ru(Tp)(dppe)\}_2(\mu\text{-adpc})]$ have been prepared and characterized. Crystal structures of $[Ru(Tp)(dppe)(Cl_5pcyd)]$ and $[\{Ru(Tp)(dppe)\}_2(\mu\text{-adpc})]$ reveal the Ru^{II} ion to occupy a pseudooctahedral coordination sphere in which the cyanamide ligand coordinates to Ru^{II} by its terminal nitrogen atom. For both complexes, the cyanamide ligands are planar, indicating significant π mixing between the cyanamide and phenyl moieties as well as the azo group in the case of $adpc^{2-}$. Spectroelectrochemistry was performed to examine the electronic absorption spectra of the $[Ru(Tp)(dppe)L]^+$ complexes. These complexes possess an intense NIR transition assigned by TD-DFT, formally, to a mixture of d−d, MLCT, and LMCT transitions because of the extensive mixing in the donor and acceptor orbitals of the scorpionate, Ru 4d, and L(NCN) orbitals. The relative oscillator strengths of this NIR band did not follow the expected trend in phenylcyanamide π-donor properties. This is due to the covalency in the ruthenium−cyanamide bond being greater with fewer chlorine substituents, as supported by DFT calculations. The noninnocence of the L(NCN) ligand was emphasized.

Spectroelectrochemistry was also performed on $[\{Ru(Tp)(dppe)\}_2(\mu\text{-adpc})]$ to generate the mixed-valence state. The intense intervalence transition that is observed in the NIR is very similar to that previously reported for $[\{Ru(trpy)(bpy)\}_2(\mu\text{-adpc})]^{3+}$ and, by analogy, identifies $[\{Ru(Tp)(dppe)\}_2(\mu\text{-adpc})]^+$ as a delocalized mixed-valence complex. This study demonstrates that it is possible to reduce the overall charge of a mixed-valence complex while still retaining the mixed-valence properties.

Future studies will attempt to synthesize neutral ruthenium(III) phenylcyanamide complexes and prepare a neutral asymmetric mixed-valence complex.

ASSOCIATED CONTENT

Supporting Information

Best fit of three Gaussian bands to the LMCT band envelope of $[Ru(Tp)(dppe)(2,3,5,6\text{-}Cl_4pcyd)]^+$, atom-labeling schemes of $[Ru(Tp)(dppe)(2,3,5,6\text{-}Cl_4pcyd)]$ and $[\{Ru(Tp)(dppe)\}_2(\mu\text{-adpc})]$, CIF files of $[Ru(Tp)(dppe)(Cl_5pcyd)]$ and $[\{Ru(Tp)(dppe)\}_2(\mu\text{-adpc})]$ crystal structures, MPA spin density of $[Ru(Tp)(dppe)(Cl_5pcyd)]$, cyclic voltammogram of $[\{Ru(Tp)(dppe)\}_2(\mu\text{-adpc})]$, and tables of DFT-optimized *xyz* coordinates, selected DFT-predicted bond distances, and TD-DFT-predicted electronic transitions. This material is available free of charge via the Internet at http://pubs.acs.org.

AUTHOR INFORMATION

Corresponding Author

*E-mail: robert_crutchley@carleton.ca (R.J.C.), blever@yorku.ca (A.B.P.L.).

Notes

The authors declare no competing financial interest.

ACKNOWLEDGMENTS

This work was supported by the Natural Sciences and Research Council of Canada and Carleton University. Computational work was made possible by the facilities of the Shared Hierarchical Academic Research Computing Network, Ontario, Canada (http://www.sharcnet.ca).

REFERENCES

(1) Marder, S. R.; Kippelen, B.; Jen, A. K.-Y.; Peyghambarian, N. *Nature* **1997**, *388*, 845.
(2) Günes, S.; Neugebauer, H.; Sariciftci, N. S. *Chem. Rev.* **2007**, *107*, 1324.
(3) Yan, L.; Wu, Y.; Hu, B. *ACS Symp. Ser.* **2010**, *1061*, 85.
(4) Creutz, C. *Prog. Inorg. Chem.* **1983**, *30*, 1.
(5) Crutchley, R. J. *Adv. Inorg. Chem.* **1994**, *41*, 273.
(6) Ward, M. D. *Chem. Soc. Rev.* **1995**, 121.
(7) (a) Mosher, J. P. M.Sc. Thesis, Carleton University, Ontario, Canada, 2001. (b) Mosher, P. J.; Yap, G. P. A.; Crutchley, R. J. *Inorg. Chem.* **2001**, *40*, 550.
(8) Mosher, P. J.; Yap, G. P. A.; Crutchley, R. J. *Inorg. Chem.* **2001**, *40*, 1189.
(9) Al-Noaimi, M.; Crutchley, R. J. *Inorg. Chim. Acta* **2007**, *360*, 3013.
(10) Trofimenko, S. *Scorpionates: The Coordination Chemistry of Polypyrazolborate Ligands*; Imperial College Press: London, 1999.
(11) De Alwis, D. C. L.; Schultz, F. A. *Inorg. Chem.* **2003**, *42*, 3616.
(12) Lever, A. B. P. *Inorg. Chem.* **1990**, *29*, 1271.
(13) Lever E_L parameters (see ref 11) were used to design the coordination sphere.
(14) Crutchley, R. J.; Naklicki, M. L. *Inorg. Chem.* **1989**, *28*, 1955.
(15) Crutchley, R. J.; McCaw, K.; Lee, F. L.; Gabe, E. J. *Inorg. Chem.* **1990**, *29*, 2576.
(16) Naklicki, M. L.; Crutchley, R. J. *Inorg. Chem.* **1989**, *28*, 4226.
(17) Aquino, M. A. S.; Lee, F. L.; Gabe, E. J.; Bensimon, C.; Greedan, J. E.; Crutchley, R. J. *J. Am. Chem. Soc.* **1992**, *114*, 5130.
(18) Linn, D. E., Jr. *J. Chem. Educ.* **1999**, *76*, 70.
(19) Alcock, N. W.; Burns, I. D.; Claire, K. S.; Hill, A. F. *Inorg. Chem.* **1992**, *31*, 2906.
(20) Buriez, B.; Burns, I. D.; Hill, A. F.; White, A. J. P.; Williams, D. J.; Wilton-Ely, J. D. E. T. *Organometallics* **1999**, *18*, 1504.
(21) Gennett, T.; Milner, D. F.; Weaver, M. J. *J. Phys. Chem.* **1985**, *89*, 2787.
(22) Evans, C. E. B.; Naklicki, M. L.; Rezvani, A. R.; White, C. A.; Kondratiev, V. V.; Crutchley, R. J. *J. Am. Chem. Soc.* **1998**, *120*, 13096.
(23) Krejcik, M.; Danek, M.; Hartl, F. *J. Electroanal. Chem.* **1991**, *317*, 179.
(24) Sheldrick, G. M. *Acta Crystallogr.* **2008**, *A64*, 112.
(25) Spek, A. L. *J. Appl. Crystallogr.* **2003**, *36*, 7.
(26) Lever, A. B. P. *Inorganic Electronic Spectroscopy*, 2nd ed.; Elsevier Publishing Co.: Amsterdam, The Netherlands, 1985.
(27) Frisch, M. J. et al. *Gaussian 09*, revisions B.01 and C.01; Gaussian, Inc.: Wallingford, CT, 2009.
(28) Dunning, T. H., Jr.; Hay, P. J. In *Modern Theoretical Chemistry*; Schaefer, H.F., III, Ed.; Plenum: New York, 1976; p 1.
(29) Hay, P. J.; Wadt, W. R. *J. Chem. Phys.* **1985**, *82*, 270.
(30) Hay, P. J.; Wadt, W. R. *J. Chem. Phys.* **1985**, *82*, 284.
(31) Hay, P. J.; Wadt, W. R. *J. Chem. Phys.* **1985**, *82*, 299.
(32) (a) Feller, D. *J. Comput. Chem.* **1996**, *17*, 1571. (b) Schuchardt, K. L.; Didier, B. T.; Elsethagen, T.; Sun, L.; Gurumoorthi, V.; Chase, J.; Li, J.; Windus, T. L. *J. Chem. Inf. Model.* **2007**, *47*, 1045.

(33) Gorelsky, S. I.; Lever, A. B. P. *J. Organomet. Chem.* **2001**, *635*, 187−196.
(34) Gorelsky, S. I. *AOMix-CDA Program*, 2005, http://www.sg-chem.net/.
(35) Mulliken, R. S. *J. Chem. Phys.* **1955**, *23*, 2338−2342.
(36) Mulliken, R. S. *J. Chem. Phys.* **1955**, *23*, 1833−1840.
(37) Mulliken, R. S. *J. Chem. Phys.* **1955**, *23*, 1841−1846.
(38) Mulliken, R. S. *J. Chem. Phys.* **1955**, *23*, 2343−2346.
(39) (a) Reed, A. E.; Curtiss, L. A.; Weinhold, F. *Chem. Rev.* **1988**, *88*, 899. (b) Glendening, E. D.; Reed, A. E.; Carpenter, J. E.; Weinhold, F. *NBO*, version 3.1, incorporated within *Gaussian 09*.
(40) Gorelsky, S. I.; Ghosh, S.; Solomon, E. I. *J. Am. Chem. Soc.* **2006**, *128*, 278.
(41) Noodleman, L.; Lovell, T.; Han, W. G.; Liu, T.; Torres, R. A. *Comprehensive Coordination Chemistry II*; Elsevier: Oxford, U.K., 2004; pp 491−510.
(42) Bickelhaupt, F. M.; Baerends, E. J. In *Reviews in Computational Chemistry*; Lipkowitz, K. B., Boyd, D. R., Eds.; Wiley: New York, 2000; pp 1−86.
(43) Stratmann, R. E.; Scuseria, G. E.; Frisch, M. J. Unpublished.
(44) Ulrich, C. *Time-Dependent Density-Functional Theory: Concepts and Applications (Oxford Graduate Texts)*; Oxford University Press: Oxford, U.K., 2012.
(45) (a) Casida, M. E.; Jamorski, C.; Casida, K. C.; Salahub, D. R. *J. Chem. Phys.* **1998**, *108*, 4439. (b) Burke, K.; Werschnik, J.; Gross, E. K. U. *J. Chem. Phys.* **2005**, *123*, 062206.
(46) Gorelsky, S. I. *SWizard program*; University of Ottawa: Ottawa, Canada, 2010; http, //www.sg-chem.net/.
(47) Zhang, W.; Bensimon, C.; Crutchley, R. J. *Inorg. Chem.* **1993**, *32*, 5808.
(48) Desjardins, P.; Yap, G. P. A.; Crutchley, R. J. *Inorg. Chem.* **1999**, *38*, 5901.
(49) Evans, C. E. B.; Ducharme, D.; Naklicki, M. L.; Crutchley, R. J. *Inorg. Chem.* **1995**, *34*, 1350.
(50) Cramer, C. J. *Essentials of Computational Chemistry: Theories and Models*, 2nd ed.; Wiley: New York, 2004.
(51) (a) Gorelsky, S. I.; Lever, A. B. P. *Int. J. Quantum Chem.* **2000**, *80*, 636. (b) Gorelsky, S. I.; Lever, A. B. P.; Ebadi, M. *Coord. Chem. Rev.* **2002**, *230*, 97. (c) Gorelsky, S. I.; Lever, A. B. P. *J. Organomet. Chem.* **2001**, *635*, 187. (d) Li, J.; Xu, L. C.; Chen, J. C.; Zheng, K. C.; Ji, L. N. *J. Phys. Chem. A* **2006**, *110*, 8174. (e) Remenyi, C.; Kaupp, M. *J. Am. Chem. Soc.* **2005**, *127*, 11399. (f) Al-Noaimi, M.; El-Khateeb, M.; Haddad, S. F.; Sunjuk, M.; Crutchley, R. J. *Polyhedron* **2008**, *27*, 3239. (g) Ess, D. H.; Nielsen, R. J.; Goddard, W. A.; Periana, R. A. *J. Am. Chem. Soc.* **2009**, *131*, 11686. (h) Futera, Z.; Klenko, J.; Sponer, J. E.; Sponer, J.; Burda, J. V. *J. Comput. Chem.* **2009**, *30*, 1758.
(52) EMSL Basis Set Exchange, https://bse.pnl.gov/bse/portal.
(53) (a) Rezvani, A. R.; Bensimon, C.; Cromp, C.; Reber, C.; Greedan, J. E.; Kondratiev, V. V.; Crutchley, R. J. *Inorg. Chem.* **1997**, *36*, 3322. (b) Evans, C. E. B.; Yap, G. P. A.; Crutchley, R. J. *Inorg. Chem.* **1998**, *37*, 6161.
(54) Begum, R. A.; Farah, A. A.; Hunter, H. N.; Lever, A. B. P. *Inorg. Chem.* **2009**, *48*, 2018.
(55) (a) Sondaz, E.; Gourdon, A.; Launay, J.-P.; Bonvoisin, J. *Inorg. Chim. Acta* **2001**, *316*, 79. (b) Fabre, M.; Jaud, J.; Hliwa, M.; Jean-Pierre Launay, J.-P.; Bonvoisin, J. *Inorg. Chem.* **2006**, *45*, 9332.
(56) Naklicki, M. L.; Gorelsky, S. I.; Kaim, W.; Sarkar, B.; Crutchley, R. J. *Inorg. Chem.* **2012**, *51*, 1400−1407.
(57) Barriére, F.; Camire, N.; Geiger, W. E.; Mueller-Westerhoff, U. T.; Sanders, R. *J. Am. Chem. Soc.* **2002**, *124*, 7263.
(58) The EPR spectrum of $[\{Ru(trpy)(bpy)\}_2(\mu\text{-}Cl_2adpc)]^{3+}$ at 10 K shows an intense radical signal with *g* components of 2.16, 2.00, and 1.96, suggesting mostly metal character. Kaim, W. Personal communication, Aug 17, 2012.